*J. King Saud Univ.*Vol. 16, *Eng. Sc* (1), 113-141, Riyadh (1424/2002)

Hybrid Coding of Images for Digital Cellular Channel

Awad Kh. Al-Asmari*, Vinay J. Singh and Subhash C. Kwatra****
**King Saud University, Electrical Engineering Department*
Riyadh, Saudi Arabia, E-mail: akasmari@ksu.edu.sa
***The University of Toledo, EECS Department,*
Toledo, Ohio 43606, USA

(Received 31 March, 2001; accepted for publication 17 September, 2002)

Abstract. In this paper, a hybrid image coding scheme is proposed for progressive transmission of images over digital cellular channels. In this algorithm the image is decomposed into multiple pyramid layers. The proposed scheme employs the concept of feedback to retrieve the information lost due to coding. The bands are transmitted according to the descending order of their respective entropies. These bands are encoded by using the vector quantization (VQ) concept. The Northern American digital cellular standard (IS-54) has been used as the wireless communication environment. Application of the proposed scheme is investigated for vehicle speeds of 0.16 km/h and 100 km/h with a channel signal-to-noise ratio of 22 dB. Simulation results using a standard test images show the significant advantage of the proposed technique over the existing algorithms in terms of the bit rate and the visual quality.

Introduction

Wireless communications have become an integral part of business and personal life in the 90s. Today, many people use cellular phone services for business and personal use. The cellular phone offers a convenient and portable communication link to just about any location. Cellular communication technologies make it possible for people to communicate on the go. Voice telecommunications has already been introduced by the mobile phone and is spreading around all over the world.

The old adage “One picture is worth a thousand words” has finally been accepted in the world of personal computing. Although the first decade of personal computing was perhaps conspicuous by the absence of image-based applications, this has rapidly changed. In fact, the number of image-based applications has probably increased at a very high rate [1]. Data communication started in the early 80’s and has been improving

ever since, but with a great drawback. Using the Public Switched Data Network (PSDN), it does not allow mobility at all. The introduction of mobility in image communications implies a move from the existing PSDN to other networks like the ones used by mobile phones.

Image data compression is crucial for transmission of images over wireless Channels. The wireless communication radio suffers from burst error in which a large number of consecutive bits are lost or corrupted by the Channel fading effect [2-4]. Typically, the bit error rate (BER) in wireless Channel ranges from 10^{-1} to 10^{-6}, which may not be acceptable for transmitting compressed images, using traditional compression schemes such as JPEG. The JPEG standard for lossy image compression using discrete cosine transform (DCT) is not very flexible for progressive transmission of images [5-6]. Therefore, it is desirable to design a robust image coding technique, which has a high compression ratio and produces acceptable image quality over a fading Channel [7-8].

The advent of hierarchical pyramid schemes for coding has enabled such transmission to be achieved in a much more logical manner. Subband coding and pyramid coding are the two candidates for progressive transmission [7]. Subband coding method has an advantage that it is critically sampled, i.e., there is no increase in the number of samples. The price paid is a constrained filter design for perfect reconstruction, which gives a relatively poor lowpass version as a coarser approximation. This is undesirable if the coarser version is used for viewing as in the case of progressive transmission. In contrast, pyramid decomposition is a redundant representation since we have a full resolution difference image. At the price of oversampling, one gains complete freedom in the design of filters. If linear filters are chosen to derive lowpass approximation in the pyramid, it is possible to select a very good lowpass filter and derive a visually pleasing coarser version. Thus, pyramid decomposition is a better choice when high visual quality must be maintained across a number of scales as in progressive transmission.

There are some studies that have been proposed in the literature for the transmission of digital images over wireless channels. Some new techniques, using Pyramid coding, for the transmission of images over the digital European cordless telecommunications (DECT) system and the CDMA-based North American digital cellular standard IS-95A have been proposed [8-11]. These techniques achieve compression rates varying from 0.125 bpp to 0.35 bpp with image quality varying from a very good coarser approximation to a near original quality image. The simulation results of these schemes are compared with the latest published algorithms over the same wireless channels and give better performance [2-3], [12].

Previous work on digital image transmission in the TDMA based IS-54 digital cellular standard environment has been investigated in [13]. Very short summary and primary results for the proposed algorithm can be found in [14].

The proposed hybrid image decomposition scheme combines the high quality pyramid decomposition scheme with the critically sampled subband coding scheme in order to provide a multiple layer of bands for progressive image transmission. Pyramid coding is applied to the input image first to obtain a visually pleasing coarser version. Secondly, subband coding splits the error image into low resolution frequency bands. This provides the flexibility of coding each band separately at different bit rates using vector quantization.

This paper is organized as follows. First, the mobile image transmission system using the IS-54 digital cellular standard is discussed. Then, the hybrid image coding scheme using vector quantization (VQ) utilizing the concept of feedback is described. The priorities of transmitting the bands on the basis of their respective entropies are also investigated. The paper concludes with the simulation results for “Lenna” and “Urban Aerial” images using the proposed hybrid image coding scheme, under vehicle speeds of 0.16 km/h and 100 km/h with channel SNR of 22 dB (which is the minimum performance requirement for the IS-54 standard under the specified channel condition with one symbol delay spread).

Mobile Image Transmission System Model

A. The IS-54 digital cellular standard

To meet the growing need of increasing the cellular capacity in high density areas, the Electronics Industries Association (EIA) and the Telecommunications Industry Association (TIA) adopted the IS-54 standard in 1992 [15]. Since there is a single analog standard in North America (AMPS), systems using IS-54 standard must operate in the same spectrum. TIA and EIA decided to make IS-54 a dual mode standard enabling it to operate in both analog and digital channels.

IS-54 provides for encoding bi-directional speech signals digitally and transmitting them over cellular and microcellular mobile radio systems. It retains the 30-KHz channel

spacing of the earlier advanced mobile telephone service (AMPS), which uses analog frequency modulation for speech transmission and frequency shift keying for signaling. Bi-directional transmissions use frequencies approximately 45 MHz apart in the band between 824 and 894 MHz. IS-54 employs time division multiple access (TDMA) by allowing three, and in the future six, simultaneous transmissions to share each frequency band. Each frequency channel provides for transmission at a digital bit rate of 48.6 Kb/s through use of differential quadrature phase shift keying (DQPSK) modulation at a 24.3 kilo baud channel rate. The channel is divided into six time slots every 40 ms. The full rate voice coder employs every third time slot and utilizes 13 Kb/s for combined speech and channel coding. The six slots provide for an eventual half-rate channel occupying one slot per 40 ms frame and utilizing only 6.5 kb/s for each call [16]. In the current IS-54 standard, each user is assigned two time slots within a frame both during downlink as well as uplink.

The IS-54 timing structure is shown in Fig. 1 [17]. The frame duration is 40ms, which is divided into six 6.67 ms time slots. Each time slot carries 324 bits; including 260 bits of user information, 12 bits of system control information (Slow Associated Control Channel-SACCH), 28 bits of time synchronization signals, and 12 bits of digital verification color code (DVCC). The remaining 12 bits are defined only in mobile to base carriers: six bits of guard time (0.123 ms) and six bits of ramp time to allow the transmitter to reach its full output power level. The synchronization bits contain a known bit pattern that a receiver uses to synchronize itself and also to train the adaptive equalizers. The system specifies six different patterns, one for each slot in a frame, which is how users can lock into time slots. DVCC bits provide the role of supervisory signals. There are 256 distinct 8-bit codes; each base station is assigned one of these codes and each receiver goes through a verification procedure, thus blocking the receiver from locking into an interfering signal from another cell.

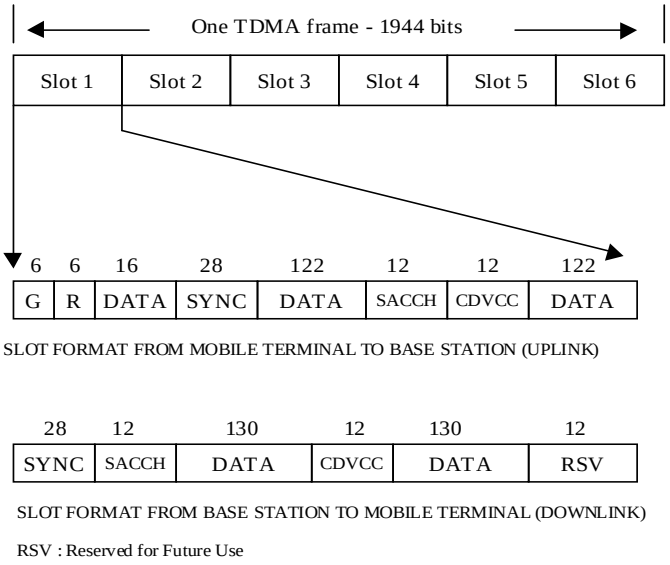

Fig. 1. The IS-54 tming structure.

B. The mobile channel and channel coding considerations

In a wireless mobile communication system, a signal can travel from transmitter to receiver over multiple reflective paths; this phenomenon is referred to as multipath propagation. The effect can cause fluctuations in the received signal's amplitude, phase, and angle of arrival, giving rise to the terminology multipath fading. A channel is referred to as frequency selective if $f_0 < 1/T_s \approx W$, where the symbol rate $1/T_s$ is nominally taken to be equal to the signal bandwidth W In practice W may differ from $1/T_s$ due to system filtering or data modulation type (QPSK, MSK, etc.). Frequency selective fading distortion occurs whenever a signal's spectral components are not all affected equally by the channel [18].

The mobile radio communication channel in urban and rural areas is typically modelled as a frequency selective multipath Rayleigh fading channel subject to log-normal shadowing [13]. One of the most popular frequency-selective fading models is the two-ray Rayleigh model. This model's instantaneous delay profile and Doppler spectra function are given by [19]:

$$c(t;\tau) = c_0(t)\delta(t) + c_1(t)\delta(\tau - \tau_1)$$

$$S_{dD}(f) = \frac{b_{00}}{\pi f_d \sqrt{1-\left(\frac{f}{f_d}\right)^2}}\delta(\tau) + \frac{b_{01}}{\pi f_d \sqrt{1-\left(\frac{f}{f_d}\right)^2}}\delta(\tau-\tau_1)$$

where $c_0(t)$ and $c_1(t)$ are subject to Gaussian distribution and f_d is the Doppler frequency.

In IS-54 the channel has been characterized as a two ray model, which are independently Rayleigh faded, with equal average power, and frequency shifted by a Doppler spread corresponding to the vehicle speed. The maximum separation between the two rays is 40 μs; i.e., one symbol time. The physical interpretation is a channel with one direct path and one reflected path with a given delay and attenuation [20]. The IS-54 standard uses ½ rate convolutional coding with a constraint length of 5 i.e. a (2,1,5) convolutional code. Interleaving the bits to be transmitted over two time slots is introduced to diminish the effects of short deep fades and to improve the error-correction capabilities of the channel coding technique. Two speech frames, the previous and the present, are interleaved so that the bits from each speech block span two transmission time slots separated by 20 ms [16]. The interleaver array has 260 elements (26 rows and 10 columns), which is the amount of data transmitted in each slot of the IS-54 frame.

The use of equalization is mandatory in IS-54. An equalizer, essentially is a filter used at the receiver end. It corrects the distortion of the received signal caused by transmission through the fading channel. In IS-54, a normal transmission burst, occupying one slot of time, contains 260 message bits with 28 bits as training sequence for the equalizer. The training sequences are designed to have impulse like autocorrelation functions, so that a simple correlation operation estimates the channel impulse response [21]. It should also be noted that adaptive equalizers also have an ability to suppress co-channel interference from other transmitters with the same bit rate [22]. An important issue in tracking the channel is whether or not one has to track during the burst. With a carrier frequency (f_c) around 900 Mhz and assuming a vehicle speed of 100 Km/hr (v), a maximum Doppler frequency of f_d = 83 Hz ($f_d = v.f_c/c$, where c is the speed of light) results. The minimum time between two fading dips is therefore roughly 6 ms (1/2 f_d [23]). In IS-54, the burst length (the duration of a time slot) is 6.7ms of the same order as the time between dips. This means that one will experience severe channel variations during the burst, thus optimized tracking algorithms are needed. Adaptive equalization is necessary to keep track of the fading channel variations and to update the equalizer parameters. In this paper, we use the Viterbi equalizer for channel equalization as proposed for frequency selective fading channels in [24]. The Viterbi equalizer used has a memory of 5 bit intervals. For each L_0-bit interval in the received message, the function of the Viterbi equalizer is to find the most likely L_0-bit sequence out of the 2^{L_0} possible sequences that might have been transmitted.

C. Block diagram of the TDMA based IS-54 digital cellular system

Based on the above discussion of the IS-54 digital cellular standard and the mobile channel, the block diagram of the mobile image transmission system is shown in Fig. 2. As we see, the block diagram represents the transmission of images over a mobile communication channel.

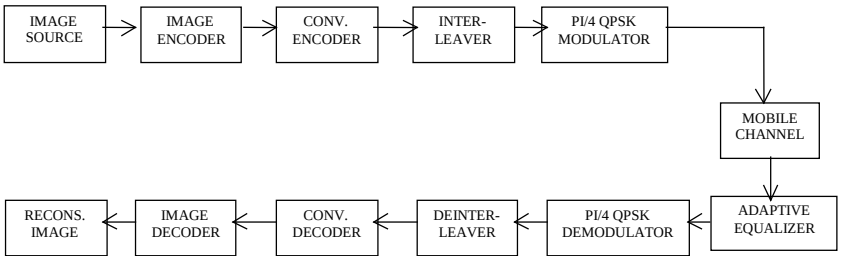

Fig. 2. Block diagram of TDMA based IS-54 digital cellular system.

The input image is compressed using the proposed hybrid image coding technique and the compressed bit stream is input to the (2,1,5) convolutional encoder. The encoded bit stream is further sent to an interleaver with 260 elements (26 rows and 10 columns). The image symbols at the output of the interleaver are truncated to an integer value and fed to a PI/4 QPSK modulator which interprets the integer value as a bit pattern to map a phase shift for the PI/4 QPSK signal. The mapping from between input data and phase shift are gray encoded so that adjacent phase shifts differ by only one bit. The output of the modulator is fed to a shaping filter having square root raised cosine frequency responses. The transfer function of the filter is given as follows:

$$|H(f)| = \begin{cases} 1, & 0 \le f \le (1-\alpha)/2T \\ \sqrt{1/2\{1-\sin[\pi(2fT-1)/2\alpha\}}, & (1-\alpha)/2T \le f \le (1+\alpha)/2T \\ 0, & f > (1+\alpha)/2T \end{cases}$$

The roll off factor determines the width of the transition band and its value is 0.35. The modulated signal is transmitted over the mobile channel and the received signal is processed by a filter matched to the pulse shaping filter. The output of the filter is further processed by the Viterbi equalizer and demodulated using the PI/4 QPSK slicer which maps the input PI/4 QPSK signal to an output signal constellation number. It uses a 1-bit differential decoder to determine the phase shift between the current input and the previous input, and then finds the nearest signal constellation point corresponding to this phase shift. The output integer values are converted to bits and fed to the deinterleaver which performs the reverse operation as that of the interleaver. The output bits are further decoded using the hard decision Viterbi decoder and are fed to the hybrid image decoder which reconstructs the received image.

Hybrid Image Coding

Signal compression needs powerful tools for information reorganization; such tools include predictive techniques for voice coding or DCT based coding for images or video that are now standards. For still image compression, the Joint Photographic Experts Group (JPEG) [25] standard is based on the DCT. The ITU has also proposed some compression algorithms using the DCT-based transform such as (JPEG) and moving picture experts group (MPEG) [26-27]. The cosine functions used in DCT are nearly optimal for stationary signals. However, images are rarely stationary. For this reason DCT based algorithms do not tolerate high compression ratios. The method generally used to decompose the source output is by representing the signal in terms of sinusoids. Another method of decomposing signals that has gained great popularity in recent years is the use of wavelets. Decomposing a signal in terms of its frequency components using sinusoids results in a very fine resolution in the frequency domain, down to the individual frequencies. However, the time resolution of the Fourier series representation is not very good. In a wavelet representation, we represent our signal in terms of functions that are localized both in time and frequency [5]. The wavelet transform due to the good localization in space and frequency domain of the basis functions can handle non-stationary signals; hence greater compression ratios can be obtained [28]. In 1989, Stephane Mallat [29] developed the multiresolution approach. Ingrid Daubechies [30] constructed orthonormal bases of compactly supported wavelets, which showed the link between wavelets and FIR (finite impulse response) filters. The wavelet decomposition can be implemented in terms of filters. Once we have obtained the coefficients of the wavelets, the filtering operation is similar to digital filtering.

JPEG 2000, the new ISO/ITU-T standard for still image coding, is wavelet-based compression algorithm [31]. This second generation algorithm is being designed to address the requirements of very different kinds of applications, e.g. Internet, color facsimile, printing, scanning, digital photography, remote sensing, mobile applications, medical imagery, digital library and e-commerce [32]. In [33-35], the authors have compared a set of features offered by JPEG 2000, and how well they are fulfilled, versus JPEG-LS (lossless coding of still images), MPEG-4 VTC (visual texture coding), and with the older and most widely used JPEG. The study compared the compression efficiency, the complexity, and set of supported functionalities [33-35]. However, we could not find research that used the JPEG 2000 for IS-54/IS-136 TDMA based coding technique to compare our proposed algorithm with. Moreover, to program the JPEG2000 for IS-54 channel will be very difficult and time consuming. Therefore, we compare our work with existed researches tested for the same wireless channel (IS-54).

A. Hybrid image decomposition

The concept of hybrid image decomposition is demonstrated in Fig. 3. The input image is first decomposed using pyramid coding into decimated image (baseband) and error images (high bands). The error images are further decomposed into 4 bands using

subband decomposition. Thus the hybrid image decomposition scheme exploits the advantages of both subband and pyramid coding.

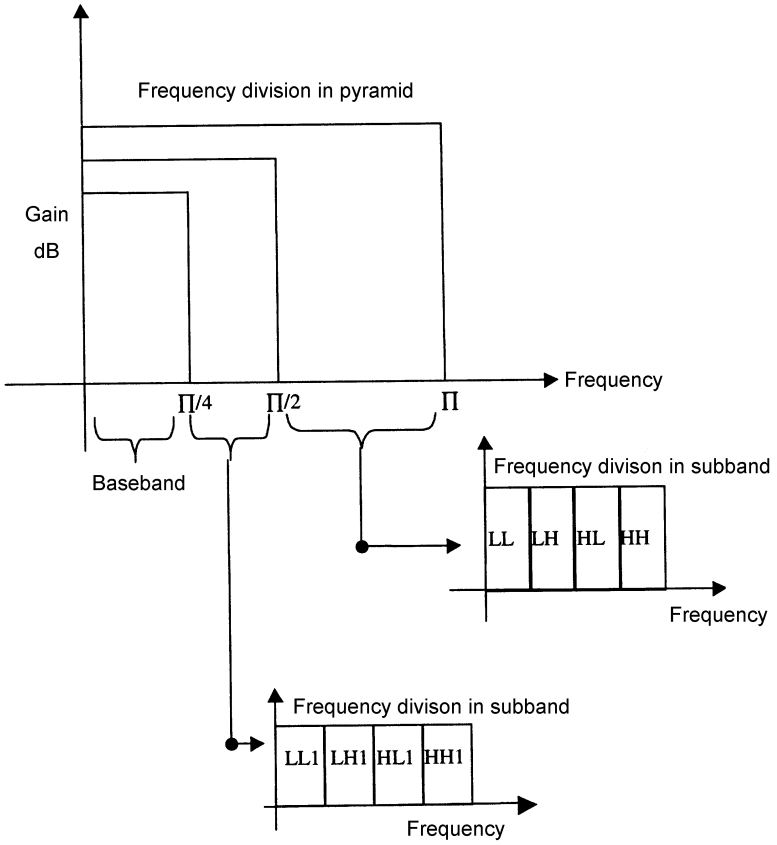

Fig. 3. Frequency division in hybrid (pyramid and subband) decomposition.

Pyramid decomposition of the input image is carried out using the 18-tap coefficients filter [5]. The 18-tap coefficients filter is selected to give a better low pass approximation of the input image. The 18-tap coefficients filter is given in Table 1. For subband coding we use the 6-tap coefficients filter bank as shown in Table 2 [5]. The 6-tap Coefficients filter exhibit the property that if the impulse response of the low pass filter is given by $\{h_n\}$, then the high pass impulse response is given by $\{ (-1)^n h_{N-1-n} \}$. The 6-tap coefficients filter is equivalent to the quadrature mirror filter (QMF) and it gives perfect reconstruction.

Table 1. 18-tap Coefficents filter for pyramid decomposition

18-tap coefficients

h_0	-.002686418671
h_1	0.005503126709
h_2	0.016583560479
h_3	-0.043220763560
h_4	-0.043220763560
h_5	0.286503335274
h_6	0.561285256870
h_7	0.302983571773
h_8	-0.058196250762
h_9	-0.050770140755
h_{10}	0.024434094321
h_{11}	0.011229240962
h_{12}	-0.006369601011
h_{13}	-0.001820458916
h_{14}	0.000790205101
h_{15}	0.000329665174
h_{16}	-0.000050192775
h_{17}	-0.000024465734

Table 2. 6-tap coefficients filter bank for subband decomposition

6-tap low pass coefficients		6-tap high pass coefficients	
h_0	-0.051429728471	h_0	-0.0110700271529
h_1	0.238929728471	h_1	0.051429972847
h_2	0.602859456942	h_2	0.272140543058
h_3	0.272140543058	h_3	-0.602859456942
h_4	-0.051429972847	h_4	0.238929728471
h_5	-0.0110700271529	h_5	0.051429728471

The hybrid decomposition scheme is applied on the standard gray scale image "Lenna" with 512 x 512 pixels having 8 bits per pixel. As shown in Fig. 4, the whole image is divided into 9 subbands. Baseband is obtained from level 2 of pyramid decomposition and has low frequency information of the image. The next 4 upper bands LL1, LH1, HL1 and HH1 are formed by subband coding the error image obtained at level 1 of pyramid decomposition and the higher 4 bands LL, LH, HL and HH are formed by subband coding the error image obtained at level 0 of pyramid decomposition. The bits are allocated based on the information content of each band. The quantitative measure of the average amount of information content of any band is the entropy of that band. The entropy of an image having gray scale values in the range 0 to 255 can be calculated using the formula:

$$H = -\sum_{i=0}^{255} P(i) \log_2 P(i).$$

where, P(i) is the probability of occurrence of a particular value [5]. Entropy of a band gives the relative importance of a band for reconstructing the image. The entropies of all the bands are listed in Table 3.

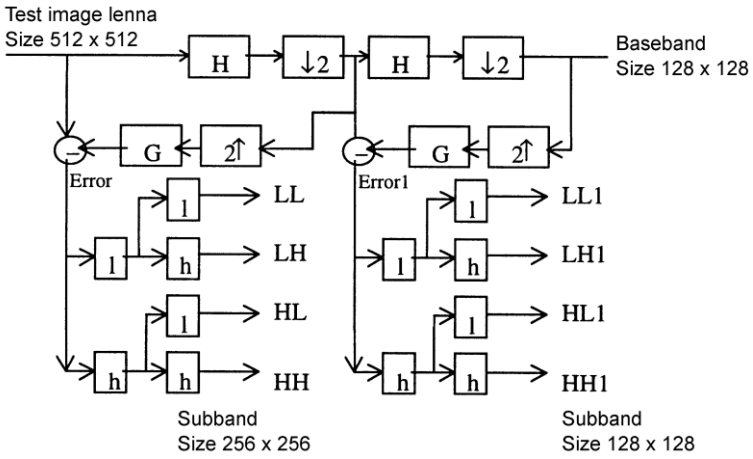

Fig. 4. Hybrid decomposition of the test image.

H : 18 – tap low pass coefficents filter for decomposition.
G : Time reversed version of the 18 – tap low pass coefficents filter for interpolation multiplied by the decimation factor 2.
↓2 : Decimation by 2.
↑2 : Interpolation by 2.
l : Low pass filtering using 6-tap low pass coefficents filter and decimation by 2.
h : High pass filtering using 6-tap high pass coefficents filter and decimation by 2.

Table 3. Entropy of the bands shown in Fig. 4

Bands	**Entropy**
Baseband	7.4313
LL1	1.8098
LH1	3.1134
HL1	3.7359
HH1	2.9362
LL	1.3107
LH	2.9307
HL	3.3566
HH	2.68

B. Coding using vector quantization

After the input image is decomposed into 9 subbands, the next most logical step is to encode the decomposed bands. The bands are coded using vector quantization. The codebooks are designed based on the information content of the bands. We have designed 4 different codebooks:

- for encoding the baseband [Codebook size 256 x 8 (block 4 x 2)]
- for encoding LL1 [Codebook size 256 x 8 (block 4 x 2)]
- for encoding LH1 and HL1 [Codebook size 256 x 16 (block 4 x 4)]
- for encoding HH1, LL, LH and HL [Codebook size 256 x 64 (block 8 x 8)]

The training set for each individual codebook is formed by taking the block of vectors from the bands that are coded using that particular codebook. The training set is formed by using five different images including Lenna image. We use the tree based splitting technique for initial codebook design. The AC energy of the vectors of the training set is used as the basic feature to divide the AC range of the training set into a prespecified number of intervals, corresponding to the number of codevectors of the desired codebook, which is determined ahead of time. The AC energy σ_x^2 of a vector X is simply the sample variance around the mean value m_x. Mathematically, these two quantities are given, respectively, by [36]:

$$m_X = \frac{1}{k} \sum_{i=1}^{k} x_i$$

$$\sigma_X^2 = \frac{1}{k} \sum_{i=1}^{k} (x_i - m_X)^2$$

The AC codebook design is the same for each codebook and uses the binary tree method. The process of designing the initial codebook is as follows [36]:

Step 1: The root node is initialised with the mean AC energy of its training set.

Step 2 : The training vectors are then divided into two halves based on their AC energy. If the AC energy of a vector is less than the mean AC value, it is placed in the left child node; otherwise it is placed in the right child node.

Step 3: Using vectors belonging to each node, the average and variance of the AC energy are computed. The variance is used to select which node to split next, while the mean AC energy is used as the split threshold.

Step 4: Repeat Step 2 and Step 3 until we have N terminal nodes i.e. the number of clusters (codebook size) is equal to the number of leaves in the tree.

Step 5: The codebook is then generated by averaging the training vectors (centroid condition) that belong to each leaf.

The initial codebook gives a very good representation of the training set which has vectors containing high frequency information. The next step is to use the popular Linde-Buzo-Gray (LBG) algorithm for fine tuning the initial codebook. Since the initial codebook is a good representation of the training set, we need to use only 3 iterations of the LBG algorithm. The steps followed in LBG algorithm are [37]:

Step 1: Begin with an initial codebook. Set m = 1.

Step 2: Given a codebook, $C_m = \{y_i\}$, partition the training set into cluster sets R_l using the Nearest Neighbor Condition (Minimum distance criteria):
$R_i = \left\{x \in \tau : d(x, y_i) \le d(x, y_j); \quad \text{all } j \ne i\right\}$

Step 3 : Using the centroid condition, compute the centroids for the cluster sets just found to obtain the new codebook, $C_{m+1}=\{\text{cent}(R_i)\}$. If an empty cell was generated in step 2, an alternate code vector assignment is made (in place of the centroid computation) for that cell.

Step 4 : Compute the average distortion for C_{m+1}. Set $m+1 \rightarrow m$ and go to Step 2.

The coupled approach of using AC based initial codebook design with LBG algorithm gives an effective codebook for coding the bands. The coding of the vectors is done on the basis of minimum distance criteria. The encoder used for VQ is based on the nearest neighbor condition. The process of decoding is very simple at the receiver, the representative index for the vector is used to pull up the vector from the codebook and is used to reconstruct the band. The block diagram of the overall coding scheme is displayed in Fig. 5. As we know that vector quantization scheme results in loss of information, we have modified our algorithm to retrieve most of the information lost during coding. The feedback scheme would be discussed in the later sections.

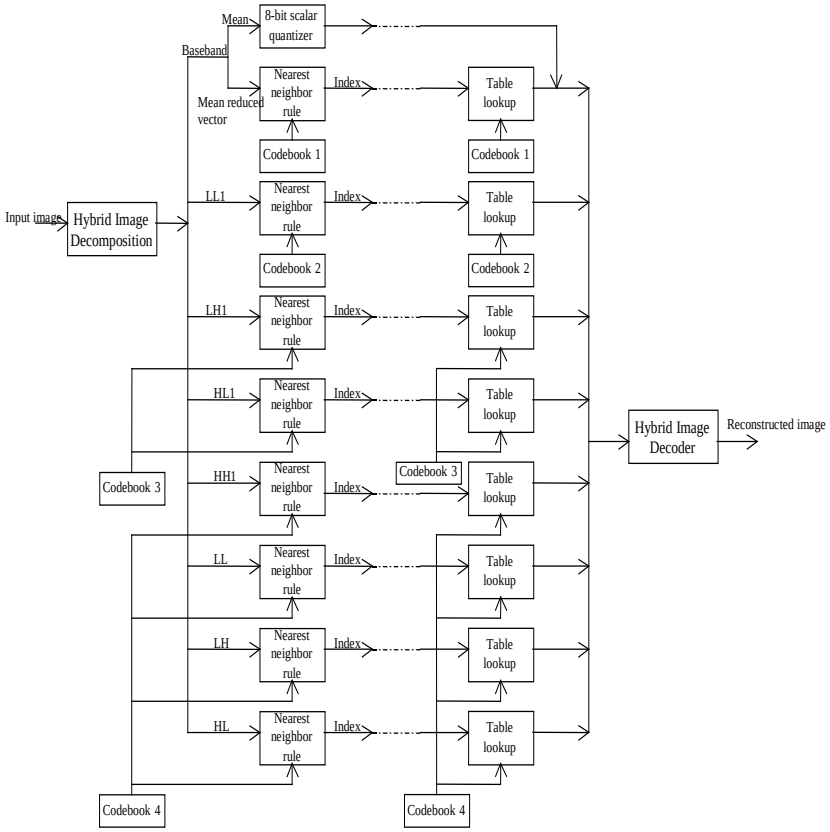

Fig. 5. Block diagram of the coding scheme.

C. Encoding the baseband

As we see from Fig. 3, baseband has low frequency information of the image, i.e., the information has a lot of DC content. To preserve the DC energy of the baseband we remove the mean of the vector and then encode the mean reduced vector using VQ. Preserving the DC energy results in better representation of the baseband using the technique of VQ. So, the baseband is encoded using "Mean Reduced Vector Quantization" (MRVQ). This technique is almost similar to VQ except that the mean of the vector is first removed and encoded separately with an 8-bit scalar quantizer, and then the mean removed vector is encoded by the VQ technique. The size of the vector depends on the image quality vs. compression tradeoff. We have selected mean reduced vector of dimension 8 picked up from the baseband as a 4 x 2 block. For an input vector of dimension 8, MRVQ coder uses 16 bits (8-bit mean & 8-bit index) reconstructing the baseband at 2 bits per pixel (16/8). As we know vector quantization is a lossy compression technique, the baseband is not reproduced exactly and some information is lost. Information lost due to coding cannot be recovered and as the baseband has the

maximum amount of information it is necessary to avoid any loss of information while coding the baseband. To retrieve the lost information we use the encoded baseband in the process of reconstruction as shown in Fig. 6. The encoded baseband is fed back instead of the baseband to obtain the error images. The information lost during encoding the baseband reflects in the error image at layer 1 of the pyramid. The entropies of the decomposed bands before and after coding are shown in Table 4. The entropy of the bands LL1, LH1, HL1 and HH1 increases after feedback as compared to the one before feedback. It is seen that the increase in entropy of the LL1 band is very high as compared to LH1, HL1 and HH1, as the baseband has low frequency information of the image. The LH1, HL1 and HH1 bands also show a slight increase in their respective entropies.

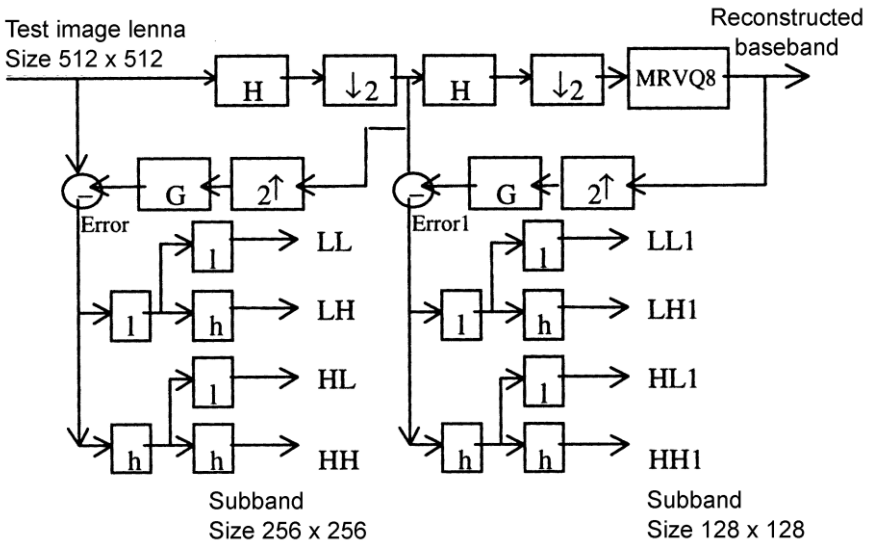

Fig. 6. Decomposed bands after the encoded baseband.

MRVQ8 : Mean reduced vector coder and decoder for baseband.

Table 4. Comparison table for entropy of the bands shown in Fig.s 4 and 6

Bands	Entropy of the bands before encoding	Entropy of the bands after the encoded baseband is fed back
Baseband	7.4313	7.4313
LL1	1.8098	4.2014
LH1	3.1134	3.2256
HL1	3.7359	3.8053
HH1	2.9362	2.9433
LL	1.3107	1.3107
LH	2.9307	2.9307
HL	3.3566	3.3566

HH	2.68	2.68

D. Encoding LL1, LH1, HL1 and HH1 bands

The entropies of the decomposed bands after feeding back the encoded baseband show the relative importance of each band. The vector dimension for each band is selected considering the most optimum compression vs. quality tradeoff. Based on the value of the entropies we select:

- Vector of dimension 64 (8 x 8 block) for HH1 band.

For the time being training set for codebook of HH1 is constructed by the vectors of dimension 64 picked up from HH1 band only. All the three codebooks are designed using the AC based tree and LBG algorithm as discussed above. Using VQ,

- LL1 band is reconstructed using 1 bit per pixel (8/8).
- LH1 band is reconstructed using 0.5 bit per pixel (8/16).
- HL1 band is reconstructed using 0.5 bit per pixel (8/16).
- HH1 band is reconstructed using 0.125 bit per pixel (8/64).

The feedback of the reconstructed baseband shows the amount of information loss because of applying lossy coding scheme to the bands. Extending the technique of feedback to the reconstructed subbands, we modify the hybrid image decomposition scheme as shown in Fig. 7. The entropies of the decomposed bands with feedback shown in Fig. 7 are listed in Table 5. The same pattern of increase in entropy is observed for LL, LH, HL and HH bands as was observed for the LL1, LH1, HL1 and HH1 bands, when we feedback the encoded baseband. The LL band reflects the low frequency information lost while coding the baseband and subbands. The LH, HL and HH bands show a very slight increase in their entropies indicating that the loss of high frequency information during coding is not substantial.

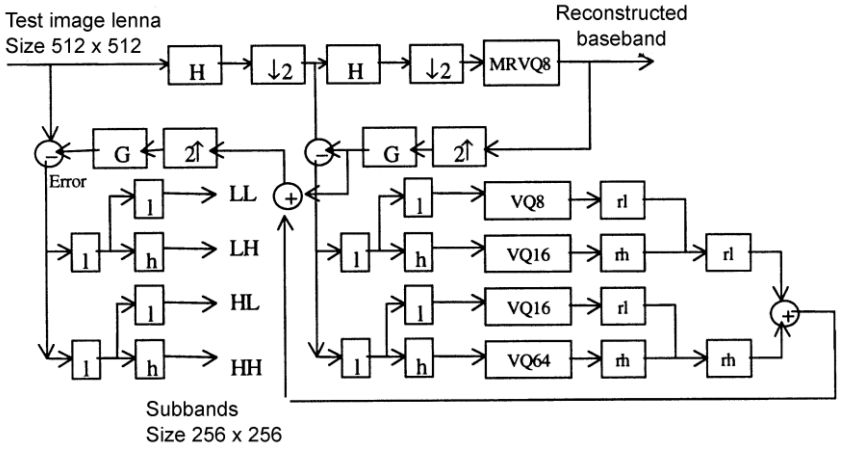

Fig. 7. Decomposed bands after encoding baseband, LL1, LH1, HL1, HH1.

rl : Interpolating the image by factor of 2 and then low pass filtering using time reversed version of 6-tap low pass coefficents filter multiplied by the decimation factor 2.

rh : Interpolating the image by factor of 2 and then high pass filtering using time reversed version of 6-tap high pass coefficents filter multiplied by the decimation factor 2.

VQ8 : Vector coder and decoder for LL1 band.
VQ16 : Vector coder and decoder for LH1 and HL1 band.
VQ64 : Vector coder and decoder for HH1 band.

Table 5. Comparison table for entropies of the subbands shown in Figs. 4, 6 and 7

Bands	Entropy of the bands before encoding	Entropy of the bands after the encoded baseband is fed back	Entropy of the bands after the encoded baseband, LL1, LH1, HL1 and HH1 are fed back
Baseband	7.4313	7.4313	7.4313
LL1	1.8098	4.2014	4.2014
LH1	3.1134	3.2256	3.2256
HL1	3.7359	3.8053	3.8053
HH1	2.9362	2.9433	2.9433
LL	1.3107	1.3107	4.1957
LH	2.9307	2.9307	3.0688
HL	3.3566	3.3566	3.4569
HH	2.68	2.68	2.6888

E. Encoding LL, LH and HL bands

The entropies of the bands again act as an indicator for the selection of vector dimension for VQ. Considering the compression vs. quality of picture tradeoff it was decided that HH band would not be transmitted and the LL, LH, and HL bands would be encoded using vector of dimension 64, reconstructing the bands at 0.125 bit per pixel. The codebook was designed using the AC based tree and LBG algorithm as discussed above. The Figs. 4, 6 and 7, along with Tables 3, 4, and 5 demonstrate the logical flow in which the hybrid image coding scheme has been developed. The block diagram of the overall hybrid image coding scheme is shown in Fig. 8.

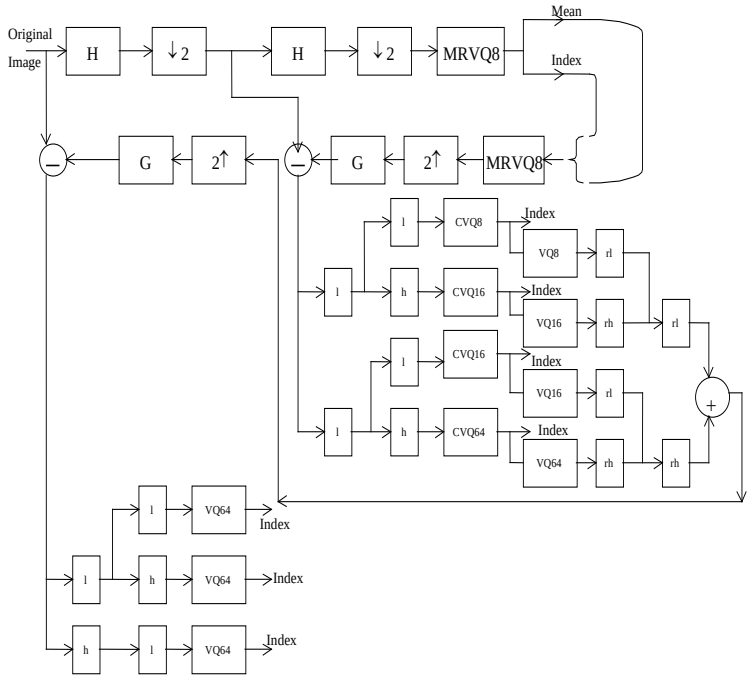

Fig. 8. Block diagram of the hybrid image coder using VQ.

F. Priority of bands for progressive transmission

The entropy of a band is a measure of the average amount of information present in that band. Thus, entropy can be used to determine the priority of the bands for progressive transmission. Arranging the entropy of all bands in a descending manner, we get the relative importance of each band. This gives the sequence in which the bands need to be transmitted. Table 6 shows the arrangement of the bands in their respective priorities. Based on the priority for progressive transmission of the bands shown in Table 6, the block diagram of the hybrid image decoder is shown in Fig. 9.

Table 6. Sequence in which the bands need to be transmitted

Sequence in which the bands need to be transmitted	Bands	Entropy of the bands arranged in a descending manner
1	Baseband	7.4313
2	LL1	4.2014
3	LL	4.1957
4	HL1	3.8053
5	HL	3.4569
6	LH1	3.2256

7	LH	3.0688
8	HH1	2.9433

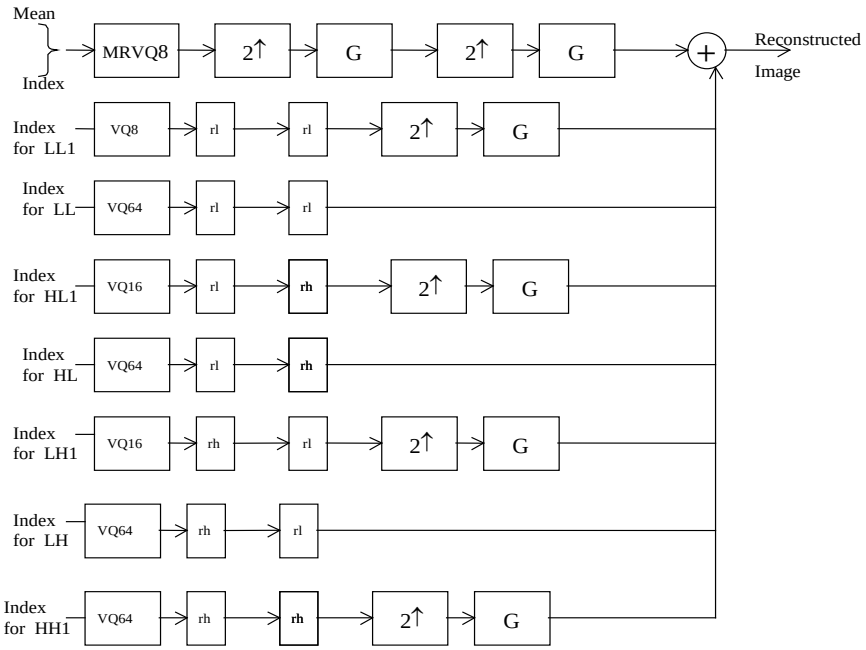

Fig. 9. Block diagram of hybrid image decoder using VQ.

Without the feedback scheme, the priority of the bands have baseband at first priority, HL and HL1 pyramid layer second priority, LH and LH1 pyramid layer third priority, HH and HH1 pyramid layer fourth priority and LL and LL1 pyramid layer as the last priority. The priority of the bands shows a very distinct behavior in terms of multi-layer arrangement of the hybrid structure. Hybrid structure brings out the concept of multiple pyramid layers. After the feedback scheme the priority of the bands change as shown in Table 5. The first pyramid layer is formed with LL at level 0, LL1 at level 1 and baseband at level 2. The second pyramid layer is formed with HL at level 0 and HL1 at level1. The third pyramid layer is formed with LH at level 0 and LH1 at level 1. The fourth pyramid layer is formed with HH at level 0 and HH1 at level 1. The priority of the pyramid layer changes with the employment of the feedback scheme.

Simulation Results

The hybrid image coding scheme has been developed and tested on some standard images such as "Lenna" image of size 512 x 512 which was among the images used in designing the codebook. To test the generality of the coding scheme we code an image outside the codebook. The other image selected is "Aerial" image of an urban area (size 512 x 512) and has characteristics different from images used in the codebook. The hybrid image decomposition technique provides for progressive transmission in multiple layers. We investigate the performance of the scheme by adding the layers in the decreasing amount of their information content. This helps to bring out the bpp (bits per pixel) vs. reconstructed image quality tradeoff. The four varying bit rates show the progressive transmission nature of the hybrid image decomposition scheme. Using the present image decomposition scheme we code the image at the following four bit rates:

- Image coding using only baseband (0.125 bpp).
- Image coding using baseband, LL1 and LL bands (0.22 bpp).
- Image coding using baseband, LL1, LL, HL1 and HL bands (0.28 bpp).
- Image coding using baseband, LL1, LL, HL1, HL, LH1, LH and HH1 bands (0.35 bpp).

The performance evaluation of the compression algorithm can be done based on mean square error (MSE), peak signal to noise ratio (PSNR) and bits per pixel (bpp) or bit rate. The MSE and PSNR are defined as follows:

$$\mathrm{MSE} = \frac{1}{m \times n} \sum_{i=1}^{m} \sum_{j=1}^{n} (X_{i,j} - \hat{X}_{i,j})^2$$

$$\mathrm{PSNR} = 20 \log_{10}\left(\frac{255}{\mathrm{MSE}}\right)$$

where, m = total number of rows, n = total number of columns, X = original pixel value and $\hat{X}$ = reconstructed pixel value. Since MSE is related to PSNR, we consider only PSNR and bit rate for our evaluation. The bit rate and the PSNR for both images are given in Table 7 and the graph for the same is as shown in Fig. 10.

Table 7. Bit rate (bpp) vs. PSNR (dB)

Bit rate (bpp)	PSNR (dB) for Lenna	PSNR (dB) for urban aerial image
0.125	27.71	25.02
0.22	29.41	26.17

0.28	31.24	26.93
0.35	32.01	27.73

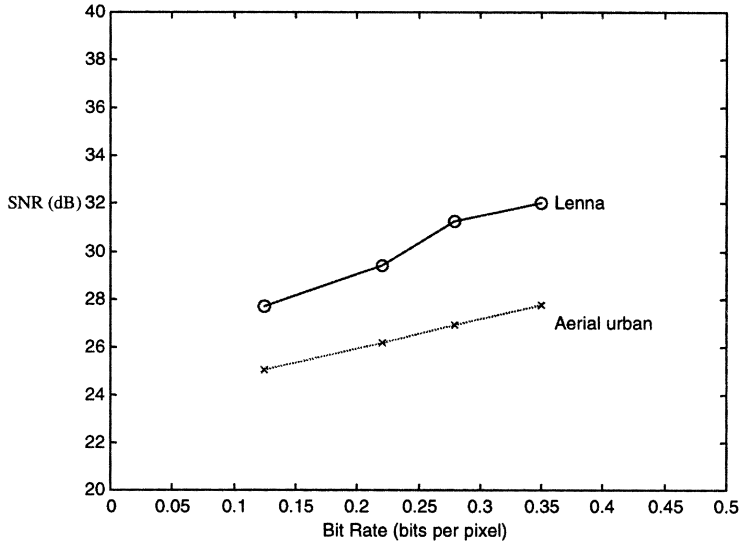

Fig. 10. PSNR vs. bit rate for lenna and urban aerial image.

From the graph we observe that as the bit rate increases the PSNR of the images also increases. The Urban Aerial image shows a linear increase in the PSNR with respect to the bit rate. The PSNR varies in the range 25-28 dB, i.e., we get an increase of 3 dB with approximately 3-fold increase in the bit rate (0.125 to 0.35). The Lenna image also shows an increasing PSNR with respect to the bit rate, but with a varying rate. The rate of increase in PSNR is more with the addition of HL1 and HL pyramid layer as compared to the other layers. The PSNR varies in the range 27-32 dB, i.e., we get an increase of 5 dB with approximately 3-fold increase in the bit rate. The original of Urban Aerial is shown in Fig. 11. The reconstructed images for Urban Aerial, at four different bit rates, are shown in Fig. 12. The reconstructed Lenna image has PSNR in the range of 27-32 dB with visual quality varying from fair to very good. The reconstructed Urban Aerial image has PSNR in the range of 25-28 dB with visual quality varying from fair to excellent quality. It is observed that the reconstructed Urban Aerial image has PSNR range less than the reconstructed Lenna image, but the visual quality is quite comparable or even better than the reconstructed Lenna image. The PSNR of the image also depends on the characteristic of the image. As Urban Aerial image has a lot of

edge details which are distorted due to compression resulting in a lower PSNR, but since these details are not easily perceptible to the human eye we get a better visual quality of the image. The reconstructed images at increasing bit rates display the gradual build up in image details as in progressive transmission of images.

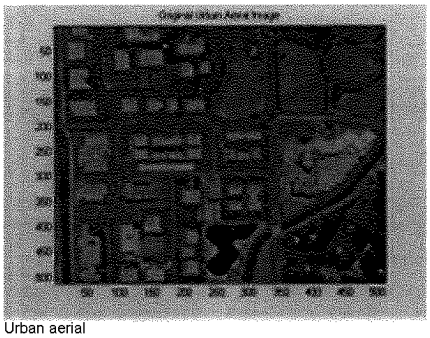

Urban aerial

Fig. 11. The original image.

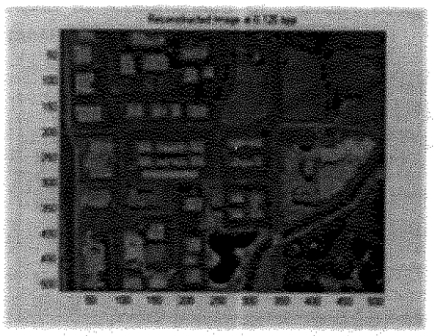

(a) Reconstructed image at 0.125 bpp.

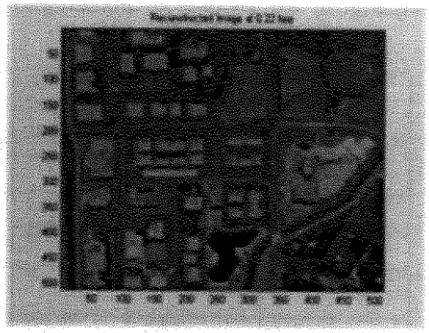

(b) Reconstructed image at 0.22 bpp.

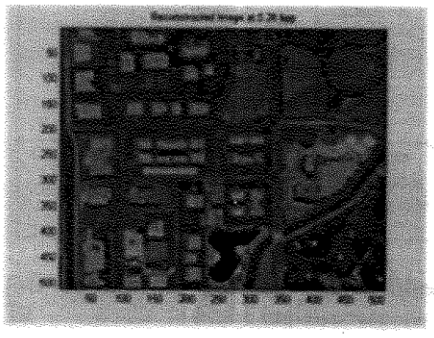

(c) Reconstructed image at 0.28 bpp.

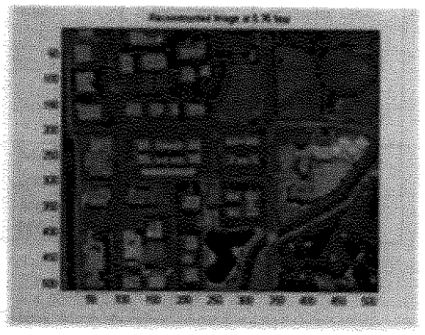

(d) Reconstructed image at 0.35 bpp.

Fig. 12. The reconstructed images for urban aerial at different bit rate (bpp).

Table 8 compares the proposed method with the existing techniques for progressive transmission. The comparison is based on the standard test image Lenna. Comparison shows that when low bit rates and moderate computational complexity are required, the choice of the proposed method is distinct. We also see that at bit rate approximately 1/3 rd of the other existing techniques the proposed method achieves competitive image quality in terms of PSNR.

Table 8. Comparison of various image compression techniques for progressive transmission

	Al-Asmari [9], 2001	**Woods and O'Neil [39], Oct. 1986**	**Al-Asmari [40], Jun 1995**	**Zhang and Liu [13], Aug. 1994**	**Proposed method**
Decomposition technique	Pyramid	Subband	Pyramid	Pyramid	Hybrid
Filter used	24-tap FIR	32-tap QMF	24-tap FIR	4-tap Wavelet	18-tap and 6-tap coefficients
Number of bands	2	16	2	7	5
Baseband coding	AMBTC	DPCM	BTC	JPEG	MRVQ
Upper band coding	MGVQ	DPCM	DCT	JPEG	VQ
PSNR (dB)	39	30.9	32.33	28.55	31.24
Bit rate (bpp)	0.69	0.67	0.875	0.29	0.28
Disadvantage	Going to high levels result in increase of bit rate.	Computation intensive.	High bit rate.	Computation intensive due to use of JPEG for all bands.	Computations at coder for vector quantization
Comments	Excellent quality at the cost of bit rate.	Moderate quality at a high bit rate.	Moderate quality at high bitrate	Low image quality at low bit rate.	Competitive quality with the lowest bit rate.

QMF : Quadrature mirror filter.
FIR : Finite impulse response filter.
DPCM : Differential pulse code modulation.
BTC : Block truncation coding.

JPEG : Joint photographic expert group standard.
DCT : Discrete cosine transform.

Table 8 compares the proposed image compression technique with the existing techniques. It is seen that the results obtained by the proposed method outperform all the other schemes both in terms of bit rate requirements as well as quality of the reconstructed image. The results obtained in [13] are comparable to the proposed method in terms of bit rate requirements but are not competitive in terms of PSNR of the reconstructed image. The PSNR obtained at 0.22 bpp with the hybrid image coding scheme is higher than the PSNR obtained at 0.29 bpp by using the image compression algorithm given in [13].

The proposed image coder is tested on the Northern American IS-54 digital cellular standard. The TDMA frame structure is shown in Fig. 1 and only the forward link, i.e., from base stations to mobile stations is considered in this paper. The test images have been compressed and reconstructed at 0.125, 0.22, 0.28 and 0.35 bits per pixel. The compressed image is transmitted over the simulated IS-54 channel. We consider vehicle speeds of 0.16 km/h and 100 km/h that represent two extreme channel conditions: stationary and rapidly time varying. A channel SNR of 22 dB is assumed since this is the minimum requirement of the IS-54 standard channel. The images are transmitted for two different channel combinations:

- IS-54 channel without FEC, i.e., the images are transmitted without onvolutional coder and interleaver.
- IS-54 channel with FEC, i.e., the images are transmitted with forward error protection using a (2,1,5) convolutional coder and interleaver. The coder along with the interleaver provides a diversity mechanism to combat the loss in PSNR.

The bit rate vs. PSNR for the various channel conditions for Lenna and Urban Aerial images is presented in Tables 9 and 10 respectively.

Table 9. Bit rate (bpp) vs. PSNR (dB) for Lenna

Bit rate (bpp)	PSNR (dB) without FEC		PSNR (dB) with FEC
	0.16 km/h	100 km/h	100 km/h
0.125	27.71	19.16	24.53
0.22	29.41	19.24	25.09
0.28	31.24	19.26	25.71
0.35	32.01	19.15	25.84

Table 10. Bit rate (bpp) vs. PSNR (dB) for urban aerial image

Bit rate (bpp)	PSNR (dB) without FEC	PSNR (dB) with FEC

	0.16 km/h	100 km/h	100 km/h
0.125	25.02	19.65	22.71
0.22	26.17	19.80	23.28
0.28	26.93	19.83	23.63
0.35	27.73	19.76	23.89

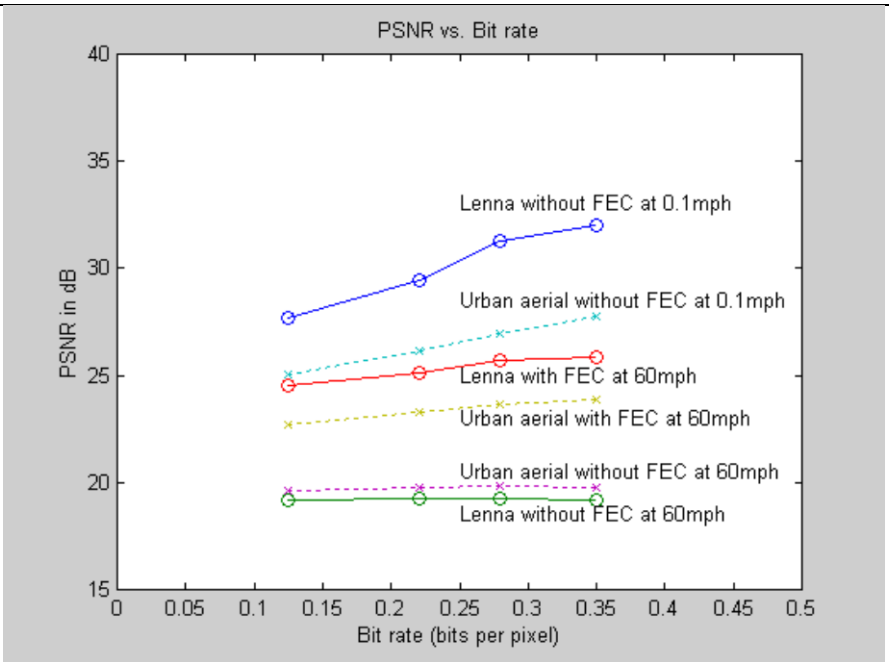

Fig. 13. The PSNR (dB) vs. bit rate for received images over IS-54 digital cellular channel.

Figure 13 displays the PSNR vs. bit rate of the received images over the IS-54 digital cellular standard. The images are received without any fading or channel distortion at vehicle speed of 0.16 km/h. The few errors that are introduced due to white Gaussian noise and fading are corrected with the help of the QPSK Viterbi equalizer used for the IS-54 digital cellular standard. The Urban Aerial image has PSNR in the range of 25-28 dB for bit rate 0.125-0.35 bpp, at vehicle speed of 0.16 km/h. The Lenna image has PSNR in the range of 27-32 dB for bit rate 0.125-0.35 bpp, at vehicle speed of 0.16 km/h. The images received without FEC at vehicle speed of 100 km/h show a sharp drop in their respective PSNR's. The PSNR for Urban Aerial image drops down to 19.8 dB approximately for bit rates 0.125-0.35 bpp. The PSNR for Lenna image also drops down to 19.2 dB approximately for bit rates 0.125-0.35 bpp at 100 km/h. This shows that the signal suffers heavy fading and distortion if forward error correction is

not employed. The images received with FEC at vehicle speed of 100 km/h show an appreciable gain in their respective PSNR's when compared to the case of reception without FEC. The PSNR for Urban Aerial image is in the range 23-24 dB for bit rates 0.125–0.35 bpp. The PSNR for Urban Aerial image increases linearly at a reduced rate. For the same bit range at 0.16 km/h the PSNR increased by 3 dB. The PSNR for Lenna image is in the range 24-26 dB for bit rates 0.125-0.35 bpp. The PSNR for Lenna image also increases at a reduced rate. For the same bit range at 0.16 km/h the PSNR increased by 5 dB. This shows that at higher vehicle speeds the rate of gain in information with increasing bit rates is lowered by the fading effect of the mobile channel.

The received images at vehicle speed of 0.16 km/h without FEC do not have any fading effect or channel distortion. The received images are the same as that shown in Figs. 12.The received images are heavily faded and distorted at vehicle speed of 100 km/h when transmitted without FEC. The reconstructed Urban Aerial image, at 0.35 bpp without FEC is shown in Fig. 14. As we can see from this Figure, Urban Aerial image is heavily distorted with patches of black and white spots. The reconstructed images at four different bit rates, for Urban Aerial when received at 100 km/h with FEC, are shown in Fig. 15. The received images show a very high reduction in fading with a few spots of fades in the overall image and the visual quality of the image increases quite significantly. The received images demonstrate the effectiveness of the FEC scheme.

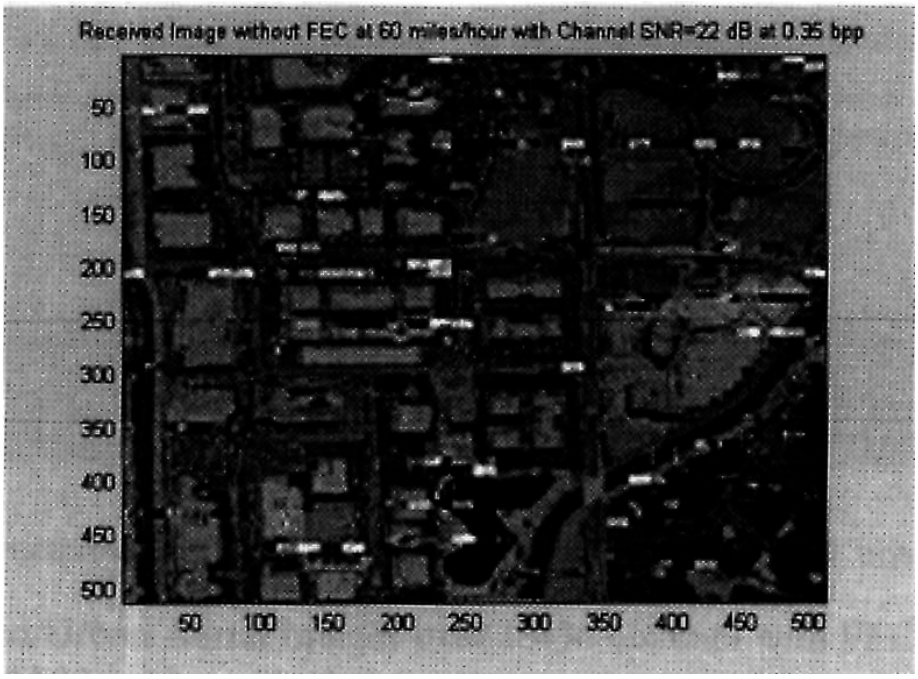

Fig. 14. The received urban aerial image at 0.35 bpp over IS-54 channel without FEC at vehicle speed of 100 km/h.

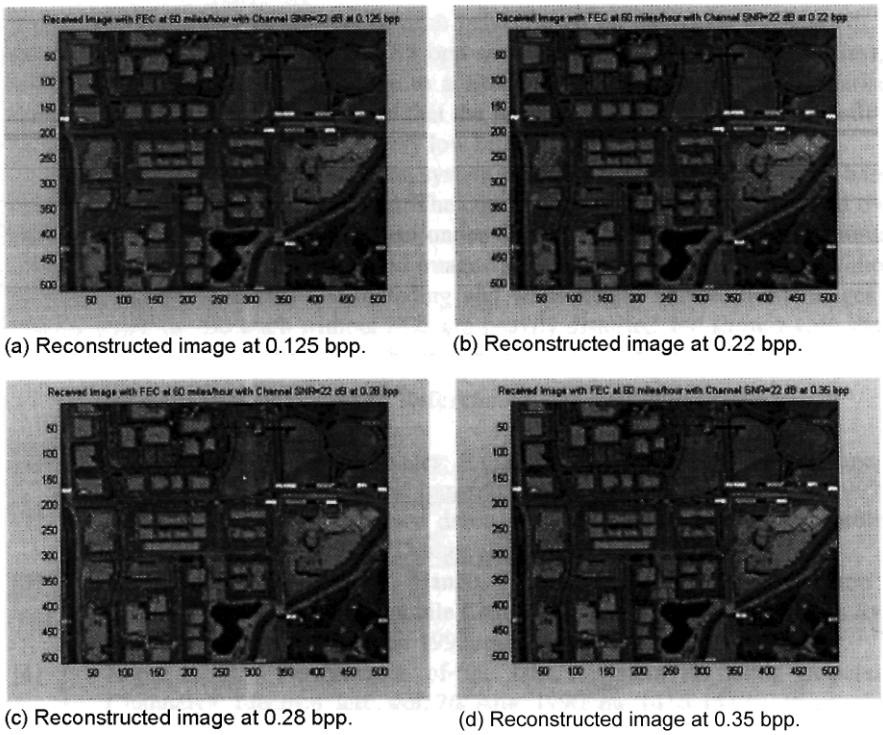

Fig. 15. Received Urban Aerial images over IS-54 channel with FEC at vehicle speed of 100 km/h.

Conclusion

A hybrid image decomposition scheme has been proposed for progressive transmission applications. 18-tap Coefficients filter is used for pyramid decomposition of the images and 6-tap Coefficients filter bank is used for subband decomposition of the error images. The images are decomposed into nine bands. The baseband is encoded using mean reduced vector quantization (MRVQ). The error decomposed bands were coded using vector quantization (VQ). The scheme developed in this research specifies the priority in which the bands should be transmitted based on the entropy of each band. Based on the bands transmitted, bit rates varying from 0.125 bpp to 0.35 bpp are obtained for the test images. Image quality varies from a blurred image to a near original

quality image. Comparison with other existing schemes, showed that the proposed scheme achieves competitive image quality in terms of PSNR at very low bit rates.

A mobile image transmission system was also presented in this paper based on the IS-54 digital cellular standard. The compressed images were transmitted over the mobile image transmission system under different vehicle speeds and minimum channel SNR of 22 dB. The received images at vehicle speed of 0.16 km/h without FEC showed no distortion due to fading and white noise. The received images at vehicle speed of 100 km/h without FEC are heavily distorted and show a very sharp drop in their respective PSNR's. The inclusion of FEC scheme at vehicle speed of 100 km/h has a very appreciable gain in the PSNR's of the received images. The simulation results show that images can be transmitted and received with acceptable image quality over mobile cellular channels.

References

[1] Held, G. *Network-based Images: A Practical Guide to Acquisition, Storage, Conversion, Compression and Transmission*. John Wiley & Sons Ltd., 1997.

[2] Fletcher, P. "DECT-standard Demo Puts Full-motion Video Over Cordless Telephone Link." *Electron. Design*, 40 (Sept. 1992), p. 34.

[3] Stedman, R., Gharavi, H., Hanzo, L. and Steele, R. "Transmission of Subband-coded Image Via Mobile Channels." *IEEE Trans. On Circuits Syst. Video Technol*, 3 (Feb. 1993), 15-26.

[4] Lops, L.B. "Performance of the DECT System in Fading Dispersive Channels." *Electron. Lett.*, 26 (Aug. 1990), 1416-1417.

[5] Sayood, K. *Introduction to Data Compression*. Morgan Kaufmann Publishers, Inc. 1996.

[6] Clarke, R. J. *Digital Compression of Still Images and Video*. Academic Press, Inc. 1995.

[7] Metin, K., Vetterli, M. and LeGall, D. "Interpolative Multiresolution Coding of ATV with Compatible Subchannels." *IEEE Trans. on Circuits and Systems for Video Tech*., 1, No. 1 (March 1991), 86-98.

[8] Al-Asmari , A. Kh. "Multiresolution Image Coding for Wireless Channel." In: *Proc. IEEE Int. Conf. on Consumer Electronics*, (June 1998), pp. 38-39.

[9] Al-Asmari, A.Kh. "Low Complexity Image Compression Algorithm for Wireless Channel." *J. King Saud Univ*., *Eng. Sci*. 13, No. 1 (2001), 85-101.

[10] Al-Asmari, A.Kh., Arya, D. and Kwatra, S.C. "Video Signal Transmission for IS-95 Environment." *Electronic Letters*, 36, No. 5 (2nd March 2000), 465-466.

[11] Al-Asmari, A. Kh., Arya, D. and Kwatra, S.C. "Transmission of Compressed Video Signal through a Spread Spectrum Channel." *Eng. Journal of Univ. of Qatar*, 14, No. 5 (2nd March 2000), 465-466.

[12] Jang, E.S. and Nasrabadi, N.M. "Subband Coding Multistage VQ for Wireless Image Communication." *IEEE Trans. Circuits Syst. Video Technol*, 5, No. 3, (June, 1995), 247-253.

[13] Zhang, Y., Liu,Y. and Pickholtz, R.L. "Layered Image Transmission over Cellular Radio Channel." *IEEE Transactions on Vehicular Technology*, 43, No. 3, (August 1994). 00-00.

[14] Al-Asmari , A. Kh., Singh, V.J. and Kwatra, S.C. "Hybrid Coding of Images for Progressive Transmission over a Digital Cellular Channel." In: *Proc. IEEE Int. Conf. on Imaging Science, Systems, and Technology*, Las Vegas, Nevada: Monte Carlo Resort, (June 28 – July 1, 1999), 120-125.

[15] EIA/TIA IS-54 Interim Standard, 1992.

[16] Gibson, J.D. *The Mobile Communications Handbook*. CRC Press , Inc., 1996.

[17] Goodman, D.J. "Trends in Cellular and Cordless Communications." *IEEE Commn. Magazine*, (June 1991), 31-40.

[18] Sklar, B. "Rayleigh Fading Channels in Mobile Digital Communication Systems Part I: Characterization." *IEEE Commn. Magazine*, (Sept. 1997), 136-146.

[19] Sampei, S. *Applications of Digital Wireless Technologies to Global Wireless Communications*. Prentice Hall, Inc. 1997.
[20] Falconer, D.D. *et al*. "Advances in Equalization and Diversity for Portable Wireless Systems." *Digital Signal Processing*, 3., No. 3 (July, 1993), 00-00.
[21] Freeberg, T. "A New Technology for High Speed Wireless Local Area Networks." *Proc. IEEE Workshop on Wireless LANs*, (May 1991), 127-139.
[22] D'Acella, R., Moreno, L. and Sant'Agostino, M. "An Adaptive MLSE Receiver for TDMA Digital Mobile Radio." *IEEE JSAC*, 7 (Jan 1989), 122-129.
[23] Proakis, J.G. Digital communications. Mac Graw Hill, 1989.
[24] Sklar, B. "Rayleigh Fading Channels in Mobile Digital Communication Systems Part 2: Mitigation." *IEEE Commn. Magazine*, (Sept., 1997), 148-155.
[25] Pennebaker, W.B. and Mitchell, J.L. *JPEG -still Image Data Compression Standards*, Van Nostrand Reinhold, 1993.
[26] Panache, P. and El Search, M. "A Look at the MPEG Video Coding Standard for Variable Bit Rate Video Transmission." *IEEE on Commun.*, (1992), 85-94.
[27] Kou, W. *Digital Image Compression Algorithms and Standards*. Boston, MA: Kluwer, 1995.
[28] Barlaud, M. "Wavelets in Image Communication. Elsevier Science B.V." *Advances in Image Commn.*, 5 (1994), 00-00.
[29] Mallat, S.G. "A Theory for Multiresolution Signal Decomposition: The Wavelet Representation." *IEEE Trans. on Pattern Analysis and Machine Intelligence*, (July, 1989), 674-693.
[30] Daubechies, I. "Time Frequency Localization Operators: A Geometric Phase Space Approach." *IEEE Trans. on Information Theory*, IT-34 (1988), 605-612.
[31] ISO/IEC/JTC1/SC29/WG1 N390R, JPEG 2000 Image Coding System, Mar.1997, http://www.jpeg.org/public/wg1n505.pdf.
[32] Charrier, M., Santa Cruz, D. and Larsson, M. "JPEG2000, the Next Millennium Compression Standard for Still Images." In: *Proceeding of the IEEE ICMCS'99*, Florence Italy, 1, No. 2 (June, 7-11), 131-132.
[33] Santa Cruz, D., Ebrahimi, T., Askelöf, J., Larsson, M. and Christopoulos, C.A. "JPEG 2000 Still Image Coding Versus other Standards." In: *Proceeding of the SPIE's 45th annual meeting*, 4115 San Diego, California: (July 30 - Aug. 4, 2000), 446-454.
[34] Santa Cruz, D. and Ebrahimi, T. "A Study of JPEG 2000 Still Image Coding Versus other Standards." In: *Proceeding of the X European Signal Processing Conference (EUSIPCO)*, Tampere: Finland, 2 (Sept. 5-8, 2000), 673-676.
[35] Santa Cruz, D. and Ebrahimi, T. "An Analytical Study of JPEG 2000 Functionalities." In: *Proceeding of International Conference on Image Processing (ICIP)*, (Jan. 2001), 49-52.
[36] Quweider, M.K. and Salari, E. "Efficient Classification and Codebook Design for CVQ." *IEEE Proceedings on Visual Image Signal Processing*, 143, No. 6 (Dec. 1996), 344-352.
[37] Gersho, A. and Gray, R.M. Ve*ctor Quantization and Signal Compression*. Kluwer Academic Publishers, 1992.
[38] Burt, P.J. and Adelson, E.H. "The Laplacian Pyramid as a Compact Image Code." *IEEE Trans. on Communications*, Com-31, No. 4 (April 1983), 532-540.
[39] Woods, J.W. and O'Neil, S.D. "Subband Coding of Images." *IEEE Trans.on Acoustics, Speech and Signal Processing*, ASSp-34, No. 5 (Oct. 1986), 1278-1288.
[40] Al-Asmari, A. Kh. "Optimum Bit Rate Pyramid Coding with Low Computational and Memory Requirements." *IEEE Trans. on Video Technology*, 5, No. 3 (June 1995), 182-192.

الترميز الهجين للصور و إرسالها عبر قناة اتصال رقمية خلوية

عوض خزيم الأسمري، فينايه جي سنقة* وسوبهاش سي كواترا*

جامعة الملك سعود، كلية الهندسة، قسم الهندسة الكهربائية،ص. ب. ٨٠٠،
الرياض ١١٤٢١، المملكة العربية السعودية
و جامعة توليدو، قسم الهندسة الكهربائية وعلوم الحاسب، توليدو،*
أوهايو ٤٣٦٠٦، الولايات المتحدة الأمريكية

(استلم في ٢٠٠١/٠٣/٣١م؛ وقبل للنشر في ٢٠٠٢/٠٩/١٧م)

ملخص البحث. تم في هذه الورقة تصميم ترميز هجين للصور الرقمية و إرسالها باستخدام مبدأ الإرسال المتتالي عبر قناة اتصال خلوية رقمية. يقوم الخوارزم المقترح بتقسيم الصورة إلى عدد من الطبقات الهرمية الشكل ومن ثم ترميزها وإرسالها. يعتمد الخوارزم المقترح على مبدأ (feedback) لكي يسهل استرجاع المعلومات المفقودة بسبب الترميز. يتم ترميز النطاقات الترددية المختلفة وإرسالها بناء على كمية المعلومات الموجودة في النطاق. حيث يتم إرسال النطاق ذو المعلومات العالية، ثم الذي يليه بطريقة تسلسلية من الأعلى إنتروبيا (Entropy) إلى الأقل إنتروبيا. يعتمد الترميز على مبدأ تكمية المتجهات (VQ).

أُستُخدِم نظام الاتصال الرقمي اللاسلكي الأمريكي والمعروف بـ (IS-54) كوسيط (قناة) اتصال لاسلكية في الاختبارات المبدئية. وقد أختبر الخوارزم المقترح عند سرعتين مختلفتين. سرعة منخفضة جدا (٠,١٦ كلم/الساعة) و عند سرعة عالية (١٠٠ كلم/الساعة). اختير نسبة الطاقة في الإشارة إلى الشوشرة في قناة الاتصال اللاسلكية بحيث تكون ٢٢ ديسي بل.

أثبتت نتائج المحاكاة على الصور المعيارية والمستخدمة في اختبارات مختلفة بأن الخوارزم المقترح يعطي نتائج أحسن من مثيلاتها من الطرق السابقة، وذلك فيما يخص معدل الإرسال وكفاءة الصورة المسترجعة.

أثبتت نتائج المحاكاة على الصور المعيارية و المستخدمة في اختبارات مختلفة بأن الخوارزم المقترح يعطي نتائج أحسن من مثيلاتها من الطرق السابقة، وذلك فيما يخص معدل الإرسال و كفاءة الصورة المسترجعة.